Published as:
Macheca AD, Focke WW, Muiambo HF, Kaci M. Stiffening mechanisms in vermiculite–amorphous polyamide bio-nanocomposites. European Polymer Journal. 2016;74:51-63. doi:10.1016/j.eurpolymj.2015.11.013

Stiffening mechanisms in vermiculite-amorphous polyamide bio-nanocomposites

Afonso D. Macheca[a,1], Walter W. Focke[a,*], Herminio F. Muiambo[a,2], and Mustapha Kaci[b]

[a]Institute of Applied Materials, Department of Chemistry and Department of Chemical Engineering, University of Pretoria, Private Bag X20, Hatfield 0028, South Africa

[b]Laboratoire des Matériaux Polymères Avancés (LMPA), Université de Bejaia 06000, Algeria

Abstract

Sub-micron thick flakes were obtained by sonication of vermiculite that was first exfoliated by either thermal shock or chemical treatment with hydrogen peroxide. Dimer fatty acid polyamide nanocomposites with a mixed morphology were prepared via a solution-dispersion technique. The large (in the micrometre range) vermiculite flakes assumed random orientations in the matrix. BET surface area measurements indicated flake thickness below 100 nm but SEM showed that thicker flakes were also present. Filler content was varied up to 30 wt.%. At this loading, the tensile strength doubled, the modulus increased five-fold but the elongation-at-break decreased by a factor of ten. Dynamic mechanical analysis suggests that three stiffening mechanisms were operating. The reinforcing effect of the high stiffness inorganic flakes is the primary contributor. Together with the chain confinement effect, that expresses itself in an apparent increase in the glass transition temperature, this provided an adequate rationalisation of the stiffness variation below *T*g. However, an additional stiffening effect is indicated at temperatures above Tg. The mechanism may involve dynamic network formation based on fluctuating hydrogen bonding interactions between the matrix polymer chains and the filler particles.

Keywords: Bio-nanocomposite; vermiculite; polyamide; mechanical properties

*Correponding author

[1]Permanent address: Department of Chemical Engineering, Eduardo Mondlane University, P.O. Box 257, Maputo, Mozambique. E-mail address: afonso.macheca@uem.mz.

[2]Permanent address: Department of Chemistry, Eduardo Mondlane University, P.O. Box 257, Maputo, Mozambique. E-mail address: hmuiambo@uem.mz.

Introduction

Polymer nanocomposites are high performance materials promising to meet new application requirements and to replace existing materials [1-3]. Adding clay-based nanoparticles can significantly improve properties such as heat resistance, stiffness, strength, toughness, impact resistance, barrier properties, rheological properties, flame retardancy, etc. [4-9]. In this regard high particle aspect ratios are desirable and are achieved by extensive delamination and even exfoliation of clay flakes. Exfoliated structures are favoured by strong interfacial adhesion and appropriate mixing processes that also effect homogeneous dispersion of clay layers within the polymer matrix [10].

Conventional polymer nanocomposites are prepared using surfactant modified clays. It is well-known that the nature of the surfactant plays an important role as it determines the degree of clay exfoliation that can be achieved. However, these surfactant molecules need to be chosen very carefully such that interaction with the polymer chains in the matrix is favoured above surfactant-clay and surfactant-surfactant interactions [8, 9]. Unfortunately the use of cationic surfactants introduces problems including limitations with respect to thermal stability. Hence surfactant-free organo-modifications are of interest [11]. In polyamides it is possible for the polymer chains themselves to provide the required organo-modification when amine functional groups are present, e.g. at the chain ends. Dimer fatty acid-based polyamides are of this type and they are soluble in lower carboxylic acids, e.g. formic acid or acetic acid [12]. When these polyamides are dissolved in acidic solvents, the amine functional groups at the ends of some chains become protonated. Thus, it is possible for these cationic polymer end groups to displace the exchangeable cations present in clays to facilitate exfoliation of the clay sheets [11]. The technique also allows organo-modification of the external surfaces of nano-sized clay sheets suspended in an acidic solution. This may facilitate clay dispersion and to prevent restacking when they are ultimately compounded into

the polymer matrix. That was one of the objectives of the present communication. However, instead of a smectite clay, submicron vermiculite nano-flakes were used. These were prepared by either first exfoliating the vermiculite via thermal shock or by suspending it in a H_2O_2 solution followed by ultrasound dispersion in the liquid phase.

The "vermiculite" of commerce features the desirable property that it expands by more than eight times in volume when heated rapidly to elevated temperatures [13-17] or by treating it with H_2O_2 [18, 19]. Heating a vermiculite flake results in the rapid transformation of the interlayer water into steam. This generates high pressure that causes the flakes to separate and to expand in a worm-like manner. This expansion can reach 30 times the original flake thickness while the original basal dimensions of the particles remain unchanged [16, 18, 20]. Vermiculite can also be exfoliated by treatment with H_2O_2 [18, 19]. Exfoliation into submicronic and even nanoflakes can be accomplished by subsequent sonication using high power ultrasound [18, 21-25].

Dimer fatty acid polyamides find application as thermoplastic hot melt adhesives and as injection mouldable polymeric encapsulants for electronics packaging [12, 26]. These applications may benefit from improvements in the matrix strength and stiffness. The present communication compares the effect of submicron vermiculite flakes, prepared by either thermal or H_2O_2 exfoliation followed by sonication, on the mechanical properties of such polyamide/bio-nanocomposites. A primary objective of the present study was to gain an understanding of the stiffening mechanisms operating in amorphous polyamide-vermiculite nanocomposites.

Experimental

Materials

Acetic acid 100% (glacial), ammonium chloride and de-ionized water were obtained from Merck Chemicals and used as received. The amorphous copolyamide, Euremelt 2138 (E2138), was supplied by Huntsman Advanced Materials. According to the supplier, this grade polyamide has a softening point in the range of 138 to 148 °C and an amine value of ca. 4 mg KOH g^{-1} polymer. Vermiculite grade Superfine (1 mm) was obtained from Mandoval Vermiculite.

Sample preparations

The raw vermiculite was first washed with de-ionized water to remove soluble compounds and organic impurities by flotation. The washed material (N-VMT) was dried at 60 °C for 48 h. The ammonium exchanged vermiculite (A-VMT) was prepared as previously described [11]. A typical procedure was as follows: Vermiculite (100 g) was suspended in 500 mL of a 1 M solution of NH_4Cl (pH ≈ 5) and stirred for 2 h at ambient conditions. The solid was separated by sedimentation and the supernatant decanted and replaced with fresh NH_4Cl solution. This procedure was repeated five times. Then the NH_4^+-vermiculite was washed with a large volume of de-ionized water until all Cl^- was removed (checked with $AgNO_3$ solution).The flakes were allowed to air dry. The resulting product was then exfoliated using either thermal shock or by suspension in a H_2O_2 solution.

Thermal exfoliation was achieved by exposing the material for 5 min to a temperature of 700 °C in a convection oven. The expanded samples were sonicated at 20 kHz and 375W using an ultrasound probe (Sonics & Materials Inc., Model Vibracell VC375, 12.15 mm diameter). Typically, 2 g of TE-VMT was suspended in 300 mL of de-ionized water and sonicated for 2 h. The slurry was allowed to settle for 2 h. Thereafter the supernatant was

decanted. Water was added to the residue and the sonication proceeded for another 2 h. This process was repeated for a third time at which stage the remaining residue was discarded. Afterwards all samples obtained in this way were combined to obtain the sonicated thermal-exfoliated vermiculite filler.

A similar procedure was used to prepare the sonicated hydrogen peroxide-exfoliated vermiculite filler. Instead of de-ionized water, 30% H_2O_2 solution was initially used as medium. The chemical exfoliation was first performed by the suspending 100 g amounts in 500 mL of 30% H_2O_2 solution at room temperature for 48 h. After the first sonication the process used for the thermal-exfoliated vermiculite was followed. The combined hydrogen peroxide exfoliated and sonicated vermiculite samples were then washed with a large amount of de-ionized water to remove any residual H_2O_2.

The sonicated vermiculite flakes were recovered by filtration and heated at 150 °C for 48 h to remove residual water. The filler powders were then re-dispersed in acetic acid at a solids content of 5 wt.%. Part of these dispersions was used to prepare polymer nanocomposites. The remaining dispersions were again washed four times with de-ionized water, dried in an air circulating oven at 60 °C for 24 h and then crushed by milling to a powder for further analysis.

A typical preparation procedure for the polyamide vermiculite composites was as follows: A weighed amount of the polyamide was separately dissolved in acetic acid, corresponding to 10 wt.% of polyamide solution. A predetermined amount of 5 wt.% vermiculite dispersion in acetic acid was placed in an 800 mL stainless steel container. It was mixed at room temperature in a high shear mixer for 2 min. Then a set amount of 10 wt.% of polyamide solution was added drop by drop. After completion of the addition, high shear mixing was continued for another 10 min. At this point the dispersion assumed a translucent appearance. Then de-ionized water was added while mixing in order to precipitate the

polymer bio-nanocomposite. The precipitate was separated from the solution by decantation. The precipitate was immersed in a large amount of de-ionized water and kept there for a total of six days in order to remove the acetic acid. The de-ionized water was replaced with fresh water on a daily basis. Following these steps, the composites were allowed to dry at ambient conditions. Finally, they were dried in a convection oven at 60 °C for 48 h. Neat polyamide polymer was also subjected to the same procedure to prepare the samples used for property comparisons. Finally, thin polymer test sheets were made by hot pressing at temperatures between 150 and 180 °C for 15 min.

Characterization

Elemental composition was determined using X-ray fluorescence (XRF) spectroscopy. Major elemental analysis was executed on fused beads using an ARL9400XP+X-ray fluorescence (XRF) spectrometer. The samples were milled in a tungsten-carbide milling pot to achieve particle sizes <75 μm and dried at 100°C and roasted at 1000°C to determine the loss on ignition (LOI) values. Then 1g sample was mixed with 6 g of lithium tetraborate flux and fused at 1050°C to make a stable fused glass bead. The Thermo Fisher ARL Perform'X Sequential XRF with OXSAS software was used for analyses.

X-ray diffraction was conducted on a PANalytical X'Pert Pro powder diffractometer with an X'Celerator detector and variable divergence and receiving slits with Fe-filtered Co-Kα radiation (λ =0.17901 nm) in the 2θ range of 2° to 60° at a scan rate of 1.0° min^{-1}.

Thermogravimetric analysis (TGA) was performed on a Perkin Elmer Pyris 4000TGA instrument using the dynamic method. About 15 mg of the sample (vermiculite or polymer) was placed in open 150 μL alumina pans. Temperature was scanned from 25 to 950 °C at a rate of 10 °C min^{-1} with air flowing at a rate of 50 mL min^{-1}.

Particle size distribution, in the range 0.01 μm to 10 mm, was determined using the low angle laser light scattering (LALLS) method on a Malvern Mastersizer 3000 instrument. The refractive indices used were 1.520 (for vermiculite) and 1.330 (for water). Specific surface area was determined using nitrogen and the BET method at liquid nitrogen temperatures with a MicrometricsTristar II BET instrument. Prior to measurements, samples were degassed under vacuum (10^{-3} mbar) at 100 °C for 24 h.

A Zeiss Ultra 55 FESEM Field emission scanning electron microscope (FESEM) was used to study the morphology of the vermiculite samples and the fracture surface morphology of the composites at 1 kV. The composite samples were frozen in liquid nitrogen, cryo-fractured and vacuum dried. The vermiculite samples and fractured surface of the composite samples were coated with carbon prior to analysis. A transmission electron microscope (TEM) (JEM-1200EX, JEOL, Tokyo, Japan) (acceleration voltage100 kV) was used to study the morphological structure of bio-nanocomposites. The samples were cry-sectioned using a diamond knife.

Melt viscosities were determined at 160 °C in the steady shear, rotational mode. An Anton PaarPhysica MCR301 rheometer fitted with a CTD 600a convection hood and fitted with a 50 mm cone-and-plate measuring system was used. The shear rate was varied from 0.1 to 10 s^{-1}.

Dynamic mechanical properties were recorded on a PerkinElmer DMA 8000 instrument. Dynamic tests were performed in the single cantilever bending mode using a displacement of amplitude of 0.05 mm at frequencies 1, 10 and 100 Hz. The sample dimensions were as follows: length = 11.30 mm, width = 4.40 mm and thickness = 2.60 mm. Temperature was scanned from −30 °C to 80 °C at a scan rate of 1 °C min^{-1}.

Tensile test specimens were punched out of the pressed sheets. They were conditioned at 25 °C and 50% RH for at least 48 h before testing. Tensile tests were performed according to

ASTM D638 at a crosshead speed of 50 mm min^{-1} on a Lloyds Instruments LRX Plus machine fitted with a 5 kN load cell. The results reported are averages of five tests per formulation.

Results and discussion

Vermiculite filler characterization

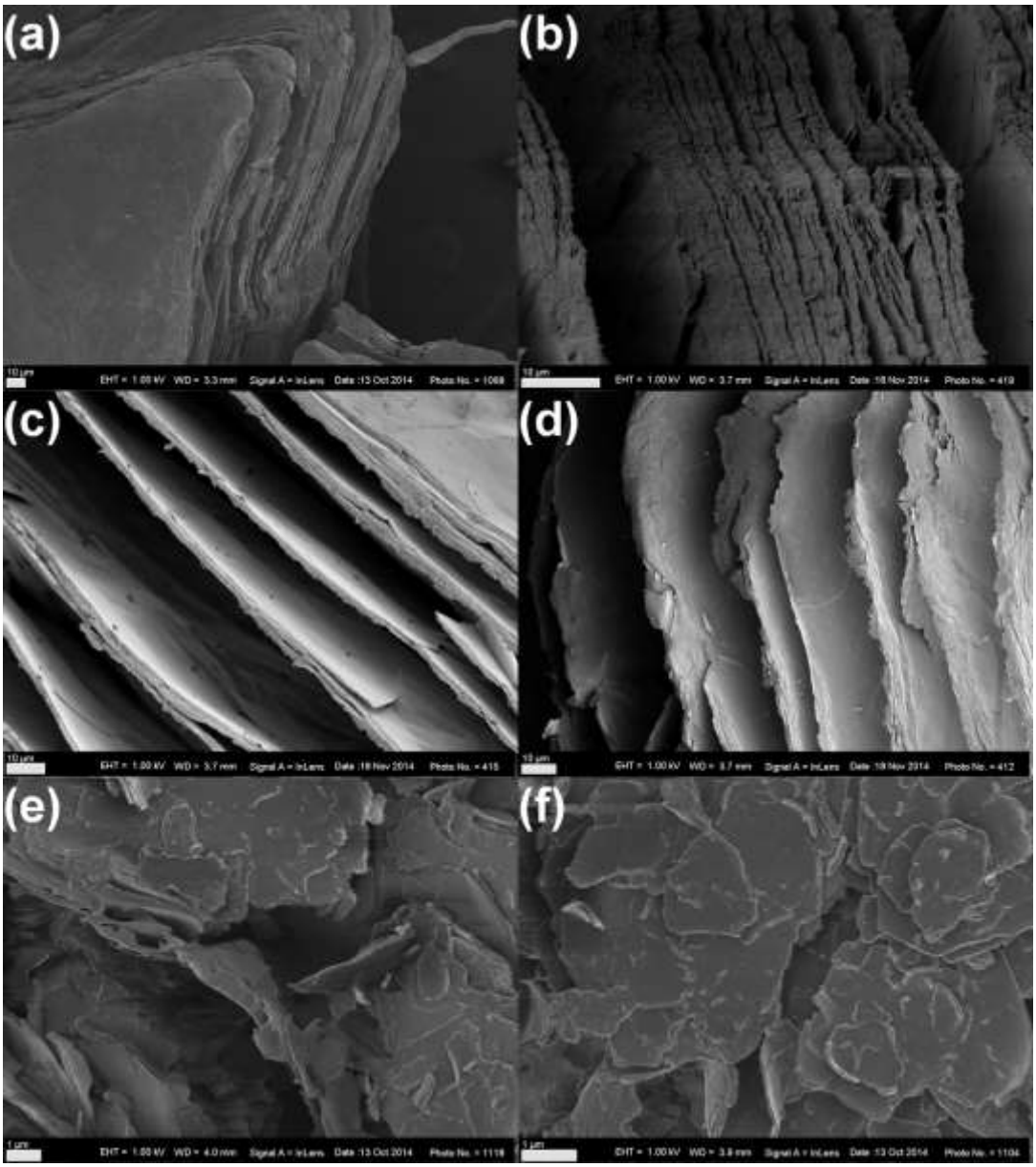

Figure 1. SEM micrographs of vermiculite samples: (a) Raw; (b) NH_4^+-exchanged; (c) H_2O_2-exfoliated; (d) Thermal-exfoliated; (e) Sonicated H_2O_2-exfoliated, and (f) sonicated thermal-exfoliated.

Scanning electron microscopy (SEM). SEM micrographs of the neat, ammonium and sonicated vermiculite flakes are shown in Figure 1. Figure 1(a) and (b) show edge-view SEM micrographs of the neat and ammonium-exchanged vermiculite flakes respectively. Figure 1(c) and (d) show the concertina-like expansion caused by a 700 °C temperature shock and chemical treatment with H_2O_2. Clearly the separation of the stacks is imperfect and the thicknesses of the flake lamellae formed are in the micrometre range, i.e. several orders of magnitude thicker than single vermiculite sheets. Figure 6(e) and (f) show that sonication led to a significant decrease of the particle sizes as observed by others [18, 25]. The majority of the particles were irregular, but on the whole, they were convex shaped two-dimensional flakes.

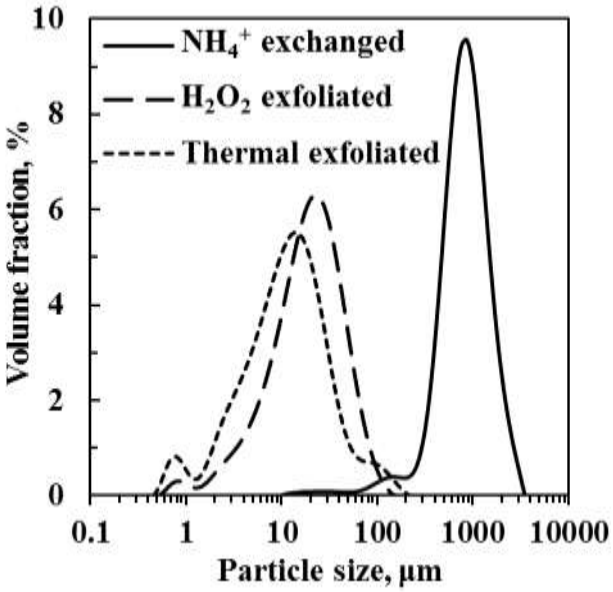

Figure 2. Particle size distribution plots of NH_4^+-exchanged vermiculites in neat pre-expanded form together with the sonicated samples that were either thermally or chemically exfoliated.

Particle size. The particle size distributions reported in Table 1 and Figure 2 confirm that ammonium exchange did not materially affect the particle size distribution. However, sonication caused a significant reduction in size. All particle size distributions showed a

bimodal dispersion with a large peak at larger size values and a much smaller peak located at lower particle sizes. Since the material consists essentially of high aspect ratio flakes, the lower humps are indicative of the variations in the flake thicknesses. In both cases the peak position is located in the sub-micron range. Table 1 indicates that the d_{50} particle size of the NH_4^+-exchanged vermiculite was 979 μm. This was reduced to 12.4 μm and 20.9 μm in the sonicated forms of the thermal- and H_2O_2-exfoliated samples, respectively. This corresponds to d_{50} size reductions of by factors of 71 and 42 for the two types. Thus, for the same conditions of sonication (frequency, power, time and temperature), size reduction was more extensive for the thermally expanded vermiculite sample than the chemically expanded sample.

Table 1: Particle sizes (μm) and BET surface areas of vermiculite samples.

Sample	**d_{10}**	**d_{50}**	**d_{90}**	**BET, $m^2\ g^{-1}$**	***t*, nm***	**λ, -#**
Neat vermiculite	423	890	1760	1.49	525	1695
NH_4^+-exchanged	421	879	1750	1.58	496	1772
H_2O_2-exfoliated	5.62	20.9	54	10.5	74	282
Thermally exfoliated	2.91	12.4	39.2	12.4	63	197

*Average flake thickness estimated from BET specific surface area. #Apparent aspect ratio estimated from d_{50}/t.

BET surface area. Table 1 also reports the BET specific surface areas for all vermiculite samples. Again, there was very little difference in the values for the raw vermiculite and the ammonium-modified version (1.49 $m^2\ g^{-1}$ versus 1.58 $m^2\ g^{-1}$). However, sonication produced a significant increase in the specific surface area to 10.5 $m^2\ g^{-1}$ for the vermiculite exfoliated by hydrogen peroxide reaction and 12.4 $m^2\ g^{-1}$ for the vermiculite exfoliated by thermal shock (Table 1). Since the surface area contributed by the edges of large aspect ratio flakes

can be neglected, this implies that the latter flakes were relatively thinner. The BET specific surface area is given by $A_{BET} \approx 2/\rho t$ where ρ is the density and t the thickness of the flakes. The average flake thickness can then be estimated from the BET surface area and the density of the vermiculite. Assuming ρ = 2.55 g cm^{-3} yields flake thickness estimates of t = 63 nm and t = 74 nm for the sonicated forms of the thermal- and H_2O_2-exfoliated forms, respectively. This suggests that the flakes may include nano-scale particles as at least one dimension was less than 100 nm. Furthermore, crude estimates of the flake aspect ratios are obtained by considering the ratio d_{50}/t. These values are also plotted in Table 1. However, these analyses did not take into account that the flakes might include lateral splits, i.e. extensive planar cracks. This means that the actual flakes could be thicker and feature lower aspect ratio values than indicated in Table 1.

X-ray fluorescence (XRF) chemical composition. The XRF chemical composition of the vermiculite samples are presented in Table 2. The values for the neat material are consistent with those previously found [14, 15]. Previous analyses established that Palabora "vermiculite" is not pure vermiculite but rather a randomly-interstratified mixed-layer vermiculite-biotite containing less than 50% vermiculite [14, 18, 27-29]. The structural formula for this mineral consistent with composition data is given in Scheme I [14]:

$$0.60\,(Mg_{2.60}Fe^{2+}_{0.60})[Si_{3.2}Al_{0.78}Fe^{3+}_{0.02}]O_{10}(OH)_2K^{+}_{0.49}$$
$$+\,0.40(Mg_{2.60}Fe^{2+}_{0.60})[Si_{3.2}Al_{0.78}Fe^{3+}_{0.02}]O_{10}(OH)_2Mg^{2+}_{0.20}.nH_2O$$

Scheme I. Structural formula for Palabora vermiculite consistent with XRF data [14].

The differences observed in the XRF analyses evident in Table 2 reflect natural variations rather than composition changes caused by the processing of the samples.

Table 2: Chemical composition (wt.%) of ignited vermiculite samples with the corresponding loss of ignition.

Sample	SiO_2	MgO	Al_2O_3	Fe_2O_3	K_2O	CaO	P_2O_5	TiO_2	LOI
Neat vermiculite	42.55	24.39	10.06	9.49	6.21	4.61	1.13	1.16	8.70
NH_4^+-exchanged	43.42	24.18	10.26	9.60	6.23	3.69	1.25	1.16	9.97
H_2O_2-exfoliated	45.67	23.02	8.67	8.62	5.34	3.95	3.48	1.02	16.3
Thermally exfoliated	43.22	23.96	9.86	9.27	5.97	4.79	1.57	1.13	19.8

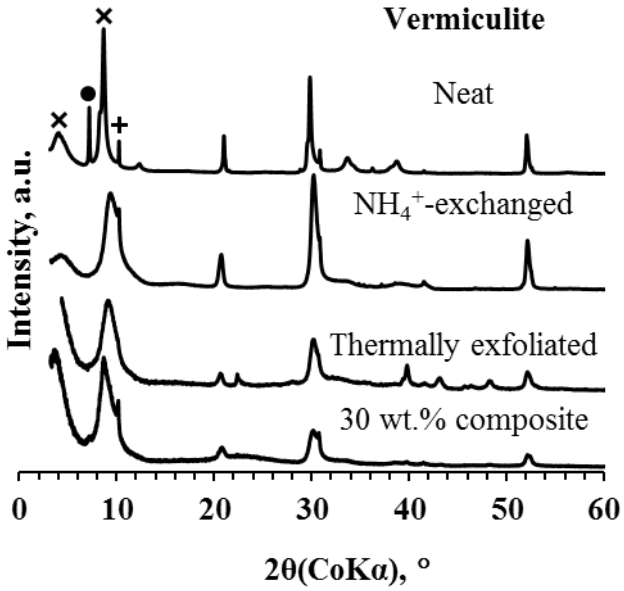

Figure 3. X-ray diffraction (XRD) patterns of the various vermiculite samples. Key: ● = vermiculite; ✖ "hydrobiotite"; and ✚mica (biotite/phlogopite).

X-ray diffraction (XRD). Figure 3 shows the X-ray diffraction (XRD) patterns of various vermiculite samples. The neat vermiculite features multiple reflections, suggesting a mixture of different minerals as reported in the literature [14, 30]. It features a strong broad peak at 2θ = 8.66° (1.19 nm) and weaker reflections at 2θ = 7.20° (1.43 nm) and 2θ = 10.24° (1.00 nm). The 1.43 nm reflection is consistent with a vermiculite phase with two water layers in the galleries forming hydration shells around the exchangeable cations [31]. The

1.00 nm reflection is from the mica (biotite/phlogopite). Perfectly alternating 50/50 mixed layered vermiculite, i.e. “hydrobiotite”, features reflections at 2.441 nm (001) and 1.221 nm (002) [32, 33]. In the present sample the main peak is located at higher 2θ angles. This and the extensive line broadening are indicative of a random distribution of the vermiculite and biotite layers.

Two XRD diffractogram sample sets corresponding to the two different exfoliation procedures were obtained. The corresponding pairs were identical indicating that similar products were obtained irrespective of whether the exfoliation was achieved through a thermal shock or hydrogen peroxide treatment. This means that the two procedures delivered similar end products as far as phase composition is concerned. Apart from the reflection intensities, the diffractograms for the composites were also independent of the concentration of the vermiculite incorporated. This was expected as the composite preparation method and the sample preparation procedure did not involve high shear forces that could have caused further delamination of the vermiculite. Therefore only the thermally exfoliated data and the diffractogram for the 30 wt.% vermiculite composite are presented in Figure 3. A broadening of the “hydrobiotite” reflections as well as the disappearance of some of them was observed in ammonium-exchanged vermiculite sample as well in the diffractograms of all the sonicated materials and the polyamide-vermiculite composites. The broadening is attributed to the delamination of vermiculite sheets together with particle size reductions induced by sonication.

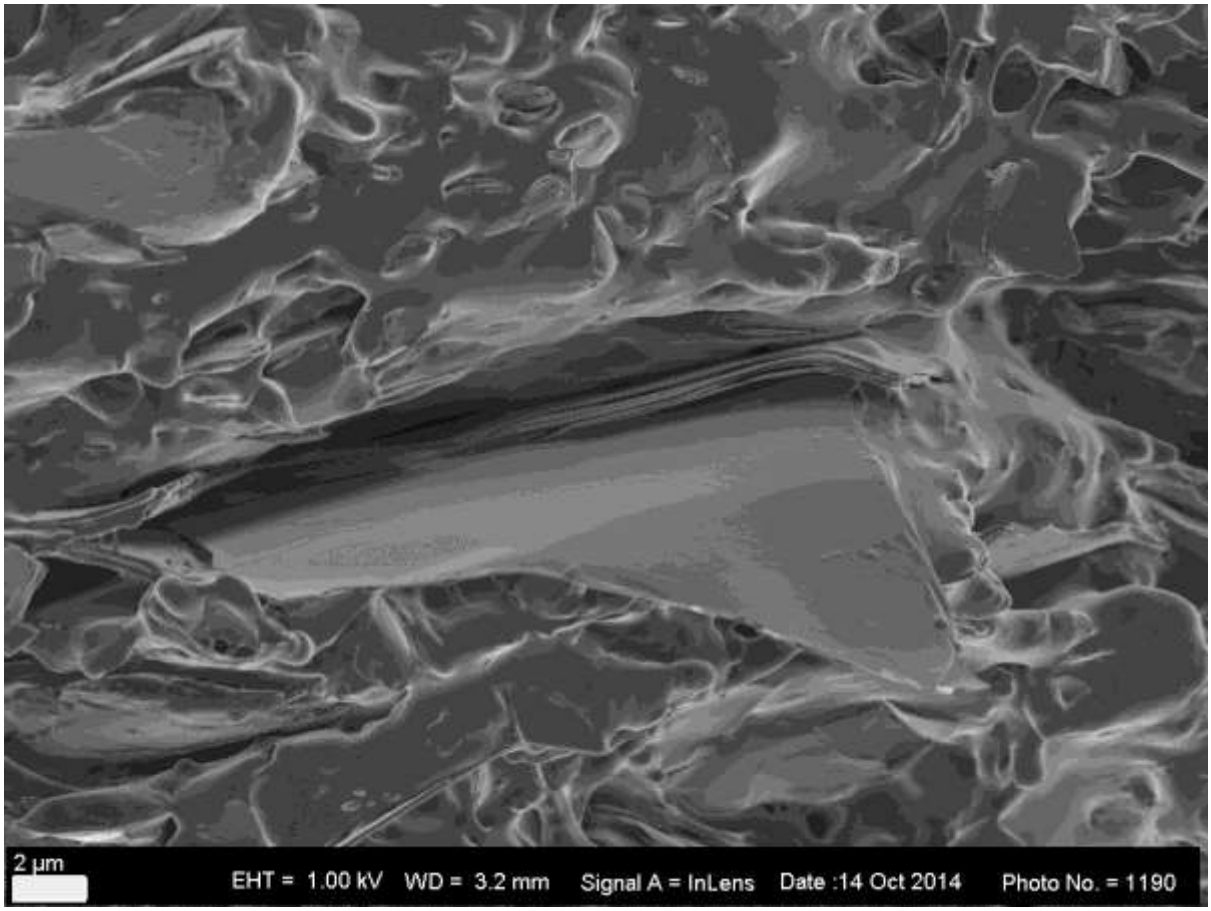

Figure 4. Cross sectional SEM image of the polyamide composite containing 20 wt.% vermiculite and (d) 30 wt.% HES-VMT content at 10 µm.

Composites characterization

Electron microscopy. Representative visualizations of the morphology and orientation of the vermiculite flakes in the polyamide composites are illustrated in Figure 4 - 6. They were obtained for sample containing 20 wt.% vermiculite obtained by sonication of exfoliated fillers. The vermiculite flakes assumed random orientations within the polymer matrix as indicated in Figure 4. However, twisted and folded platelets were also observed. TEM micrographs taken of microtome cross-sections (Figure 6) show flake thickness in the sub 100 nanometer range. However platelets with thickness up to about one micrometre are observed in SEM micrographs (Figure 4). The polyamide appears to have covered the

external surfaces of vermiculite platelets (Figure 5). This suggests good wetting and a strong interaction between the outer surface of vermiculite layers and the polyamide matrix. This is supported by the cohesive rather than adhesive failure of the matrix seen in Figure 5: Note the ropey polymer structures connecting two flakes. However, the flakes in Figure 5 also feature partial delamination, i.e. lateral internal cracks that appear to be devoid of polymer. It is considered likely that these cavities were not present initially but that they were created during the cryofracturing of the sections containing the rigid vermiculite sheets.

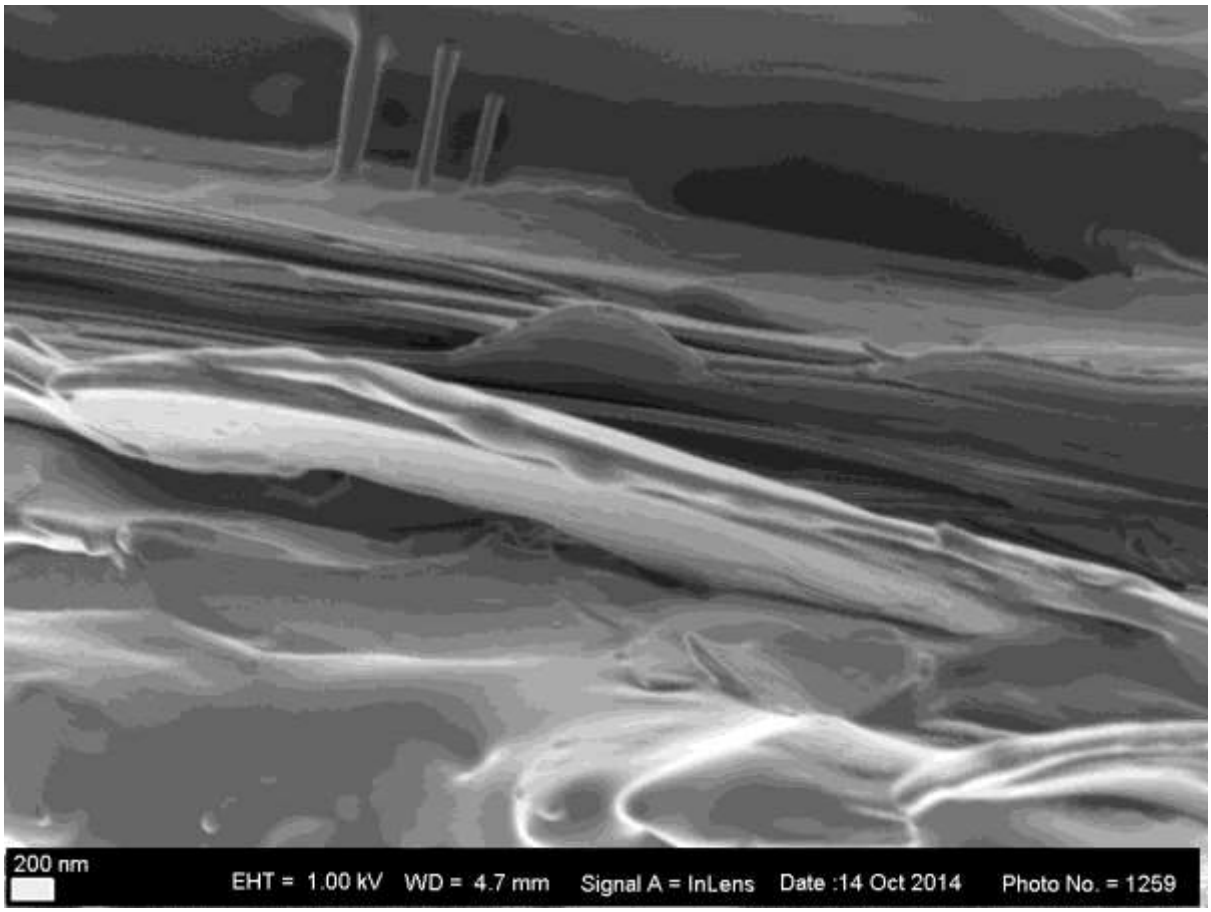

Figure 5. Cross sectional SEM images of polymer composites 20 wt.% thermally expanded vermiculite.

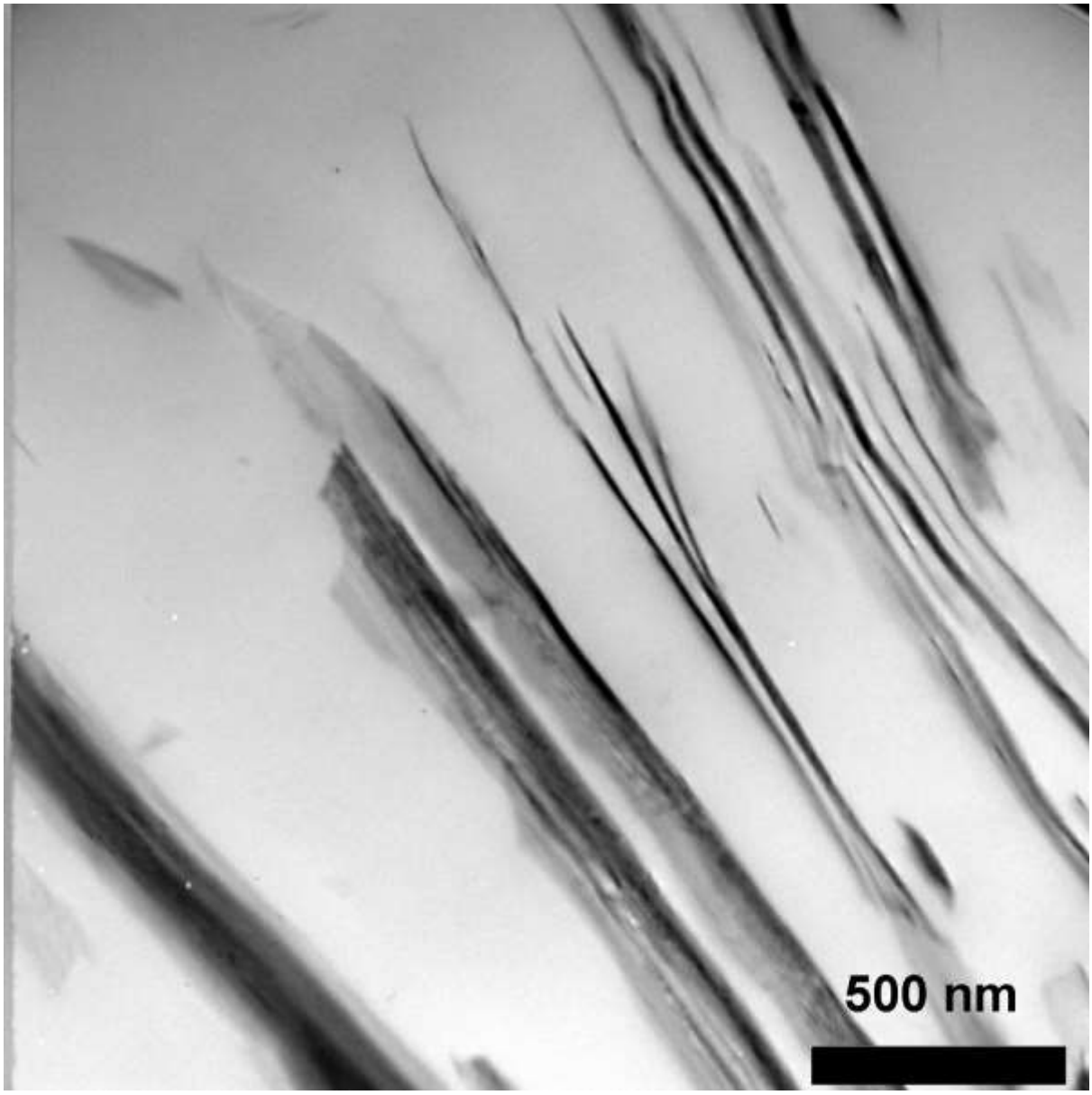

Figure 6. TEM images of polyamide composites containing 20 wt.% sonicated H_2O_2-exfoliated vermiculite.

The micrographs evidence for the composites is consistent with a filler morphology comprising a combination of nano-platelets and micro-flakes. A similar morphology was previously observed for vermiculite reinforced polyurethane [34].

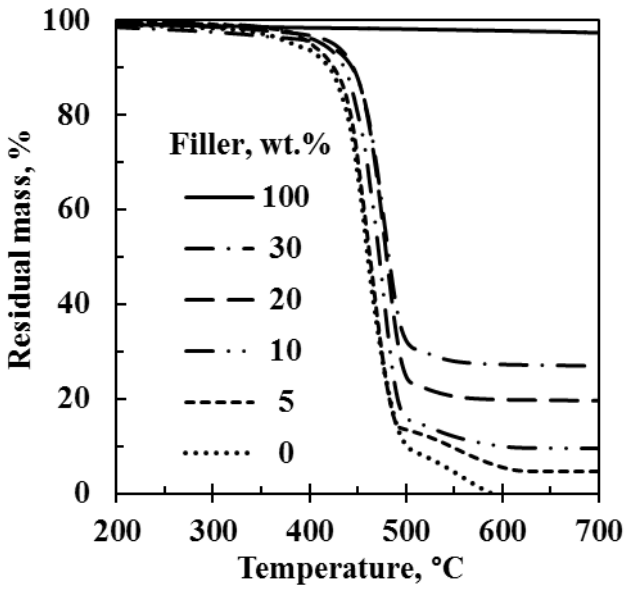

Figure 7. TGA curves for sonicated H_2O_2-exfoliated vermiculite and its polyamide composites.

Thermogravimetric analysis (TGA).TGA curves recorded in an air atmosphere for sonicated H_2O_2-exfoliated vermiculite and its polyamide composites are presented in Figure 7. The curves for the materials derived from the thermally exfoliated vermiculite have a similar appearance. Mass loss commenced below 100 °C for the NH_4^+-exchanged vermiculite and occurred in several steps. The total mass loss reached 7.6 wt.% at 950 °C. It reflects the loss of physisorbed and interlayer water at lower temperatures and mass loss due to dehydration of hydroxyl groups at elevated temperatures.

The TGA curves for the neat polymer and the composites display two major mass loss steps. Most of the mass loss occurs in the first step in the temperature range 300 °C to 500 °C. The polyamide leaves a char residue of about 10 wt.% at 500 °C and mass loss is complete at ca. 600 °C. Above this temperature the composites show plateau values corresponding to the inorganic residue derived from the decomposition of the vermiculite. These were used to confirm filler content of the composites. The first mass loss event commences at higher temperatures in the composites. This reflects the effect of the flake-

shaped filler particles that inhibit the mass transfer to the atmosphere of the volatile degradation fragments. However, a radical trapping effect may also play a role [35].

Mechanical properties. Figure 8 shows that the tensile strength increased with filler loading while the elongation at break decreased precipitously. At a loading of 30 wt.% vermiculite, the tensile strength was about double of that of the neat polyamide. However, the elongation-at-break was only one tenth of the original value.

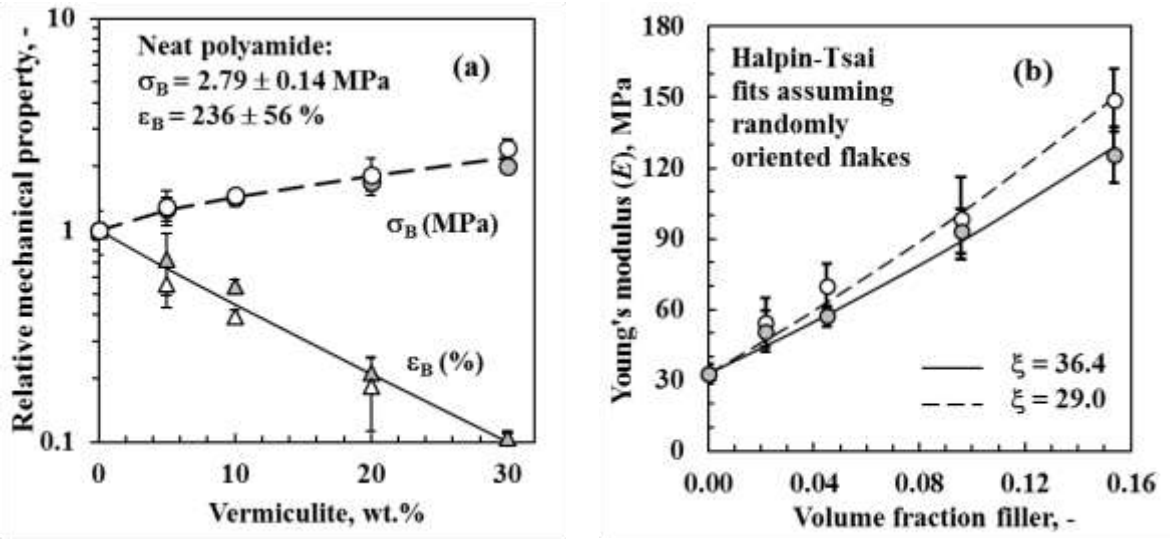

Figure 8. Effect of vermiculite content on (a) the tensile strength and elongation-at-break, and (b) the Young's modulus. Open symbols: Thermal-exfoliated vermiculite. Filled symbols: H_2O_2-exfoliated vermiculite.

Modelling the Young's modulus. The Halpin-Tsai equation [36] is widely used to predict the modulus of composites [37, 38]:

$$\frac{E}{E_p} = \frac{(1+\xi\eta V_f)}{(1-\eta V_f)} \qquad (1)$$

where E is the composite tensile modulus, E_p is the tensile modulus of the matrix, V_f is the volume fraction filler and ξ is a shape factor that depends on the geometry of the filler particles and their relative orientation with respect to the load direction. The parameter η is given by

$$\eta = \frac{(E_f / E_p - 1)}{(E_f / E_p + \xi)} \quad (2)$$

where E_f is the tensile modulus of the filler. Van Es [39] proposed corrected shape factors for platelet reinforcements for the longitudinal (E_{CL}) and transverse (E_{CT}) composite modulus as $\xi_L = \frac{2}{3}\frac{w}{t}$ and $\xi_T = 2$, respectively. Van Es [39] also approximated the composite modulus of a matrix containing randomly oriented platelets using an averaging scheme as follows:

$$E_c = 0.49E_{CL} + 0.51E_{CT} \quad (3)$$

where E_c is the composite modulus and E_{CL} and E_{CT} are evaluated from the Halpin-Tsai equations using the respective shape factors ξ_L and ξ_T.

Figure 8 shows least square fits of the Halpin-Tsai equations for platelets to Young's modulus data of the present vermiculite-based composites assuming random platelet alignment. The tensile modulus for the vermiculite flakes was taken as 175 ± 16 GPa [40]. The tensile moduli of the polyamide was taken as the measured value of 33 ± 4 MPa. By considering random orientation of the platelets and using Equation 3 with ξ_T fixed at $\xi_T = 2$, good fits were obtained using ξ_L = 29.0 and ξ_L = 36.4, for the composites based on H_2O_2-exfoliated and thermal-exfoliated vermiculite fillers respectively. These values correspond to aspect ratios of the platelets of 43.5 and 54.5.

Viscosity. The melt viscosity of filled polymer compounds is important as it relates to the processability by conventional plastic conversion technologies such as extrusion and injection moulding. The melt viscosity is sensitive to the structure, particle size and shape as well as the interface characteristics of the dispersed phase [41]. In some suitable instances, rheology can even be used to quantify the shear thinning effect for polymer–clay

nanocomposites and thereby to compare the extent of delamination of platelet stacks [42]. According to Figure 9, the neat polyamide and its vermiculite composites all showed weak shear thinning behaviour. The addition of vermiculite significantly increased the melt viscosity. For the H_2O_2-exfoliated vermiculite, at a loading of 30 wt.%, the viscosity was more than an order of magnitude higher than that of the neat polyamide.

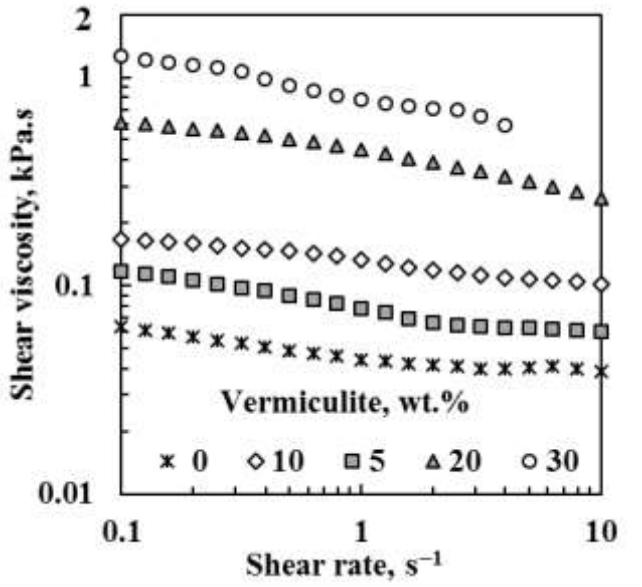

Figure 9. Effect of the vermiculite type, content and shear rate on the viscosity of polyamide composites at 160 °C. Open symbols: H_2O_2-exfoliated vermiculite. Filled symbols: Thermal-exfoliated vermiculite.

Dynamic mechanical analysis (DMA). Typical DMA results are shown in Figure 10. The glass transition temperatures for each material was associated with the position of the tan δ peak. The values are reported in Figure 11(a) as a function of filler loading and measurement frequency. The presence of the vermiculite filler caused a large upward shift of up to 10 °C in the glass transition temperature (*T*g). This shift in the glass transition temperature suggests that the presence of the filler constrained polymer chain mobility. As evidenced by Figure 10(a) and Figure 11(a), although *T*g increases with increasing vermiculite content, the composition dependence is weak. The bending modulus for the neat

polyamide shows a plateau value at temperatures well below *T*g. It decreases rapidly towards much lower values as *T*g is approached and passed. The modulus curves for the filled compounds show a similar shape. In essence they appear shifted upward and towards higher temperatures when compared to the curve for the neat polyamide. Figure 11(b) shows the effect of filler content and measurement frequency on the modulus plateau values in the glassy region. The modulus does increase slightly with frequency but filler content has a much greater effect. The reinforcing action of the stiff inorganic flakes is the primary reason for the increase in the bending modulus. However, the increased *T*g values for the polymer matrix also contributes. These two effects were removed by scaling the modulus curves and plotting them with respect to the temperature shift relative to the corresponding glass transition temperatures. Such master curves are plotted in Figure 12. They show that, for all practical purposes, this curve shifting approach collapsed all the data sets into a single curve for temperatures below *T*g. This implies that, in the glassy region, the reinforcing action of the filler is adequately described by a combination of filler micro-mechanics (the primary effect) and a secondary effect associated with the reduction in chain mobility caused by the special confinement effect imposed on the polymer chains by the high surface area flakes. The latter expresses itself by a change in the effective thermal state of the polymer chains that is adequately captured by the apparent shift in the glass transition temperature (*T*g).

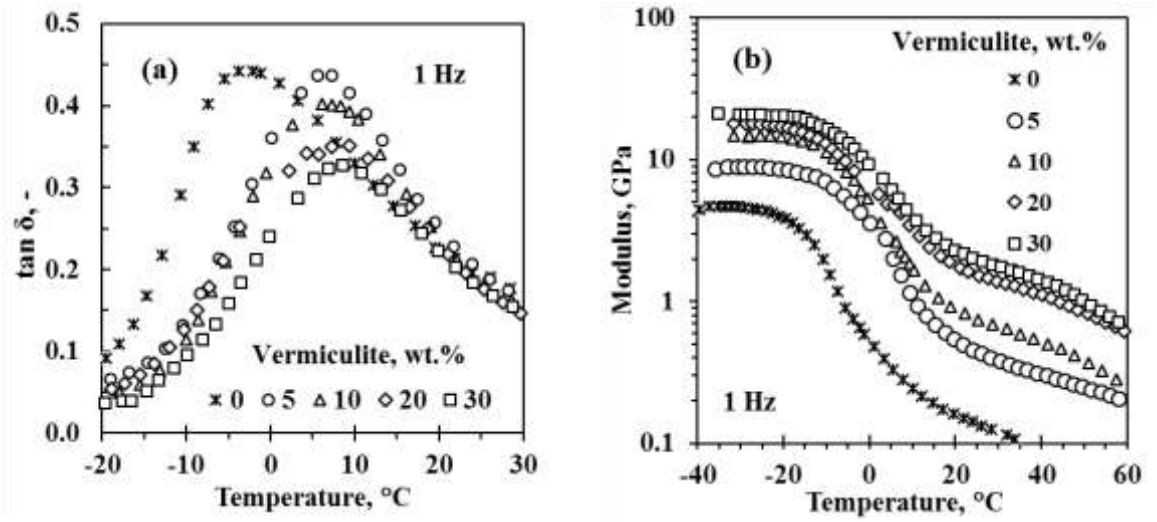

Figure 10. Representative plots showing the effect of filler loading on (a) tan δ, and (b) the storage modulus (bending mode) at a frequency of 1 Hz. The filler was sonicated thermal-exfoliated vermiculite.

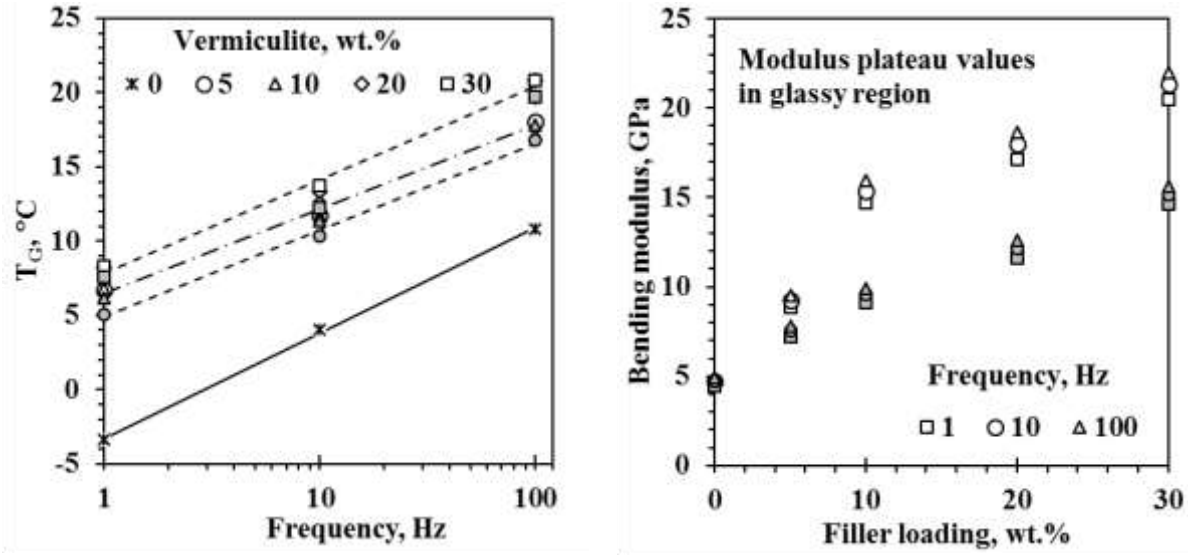

Figure 11. The effect of filler loading on (a) the glass transition temperature (from tan δ plots), and (b) the storage modulus (bending mode). Open symbols: Thermal-exfoliated vermiculite. Filled symbols: H_2O_2-exfoliated vermiculite.

Significant deviations are apparent at temperatures above *T*g with the modulus values failing to form a single band. The scaled modulus curves deviate to higher values as the filler content is increased. Compared to the curve associated with the neat polyamide, the moduli

decrease more slowly with increasing temperature. Nevertheless, the curves for compositions containing 20 wt.% and 30 wt.% filler virtually coincide. This means that there must be a tertiary reinforcing effect attributable to the presence of the flakes that reaches a limit beyond which further addition of filler has little effect.

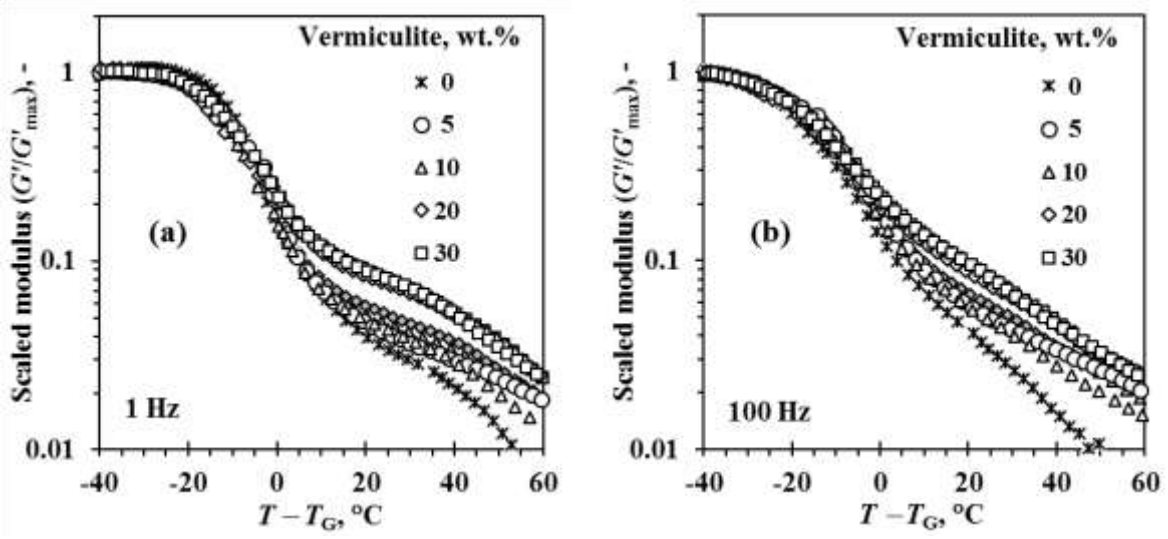

Figure 12. Modulus "mastercurves" generated by scaling with respect to the modulus plateau in the glassy region and a glass transition temperature shift. The glass transition was associated with the temperature corresponding to the peak in tan δ. Open symbols: Thermal-exfoliated vermiculite. Filled symbols: H_2O_2-exfoliated vermiculite.

It is tentatively proposed that virtual crosslinking forms the basis of this tertiary effect. The electron microscopy results have confirmed strong interactions between the polyamide matrix and the vermiculite flake surfaces. That was expected given that, by design, some polymer chain ends are attached to the mineral surface via strong electrostatic forces. Furthermore, the polyamide chains are capable of strong inter-chain hydrogen bonding interactions as well as interactions with the vermiculite surfaces, whether covered by polymer or not. Above the glass transition temperature the chains have considerable mobility. The dynamic nature of hydrogen bond formation creates a time-varying and spatially fluctuating cross-linked network that connects chains and filler particles. The effective crosslink density

of these networks is increased as the filler content increases. Increased crosslink density implies increased stiffness of the network explaining the higher modulus values at elevated temperature observed in Figure 12. Strong interactions between reinforcement and matrix molecules originated from hydrogen bonding were previously observed in dimer acid polyamide filled with cellulose fibres [43].

Conclusions

Submicron vermiculite flakes bio-nanocomposites were prepared via a solution-dispersion procedure designed to effect in situ organo-modification of the filler surface by protonated dimer fatty acid polyamide chains. Bio-nanocomposites, based on a dimer fatty acid polyamide, were successfully prepared from ammonium ion-exchanged vermiculite. The flake-like reinforcement was generated by first exfoliating the mineral via either thermal shock or treatment with hydrogen peroxide followed by sonication. This resulted in extensive delamination and size reduction. The matrix vermiculite compatibilisation did not employ any surfactants. The composites were made by mixing an acetic acid dispersion of vermiculite flakes with a solution of the polyamide in the same solvent. The composite was recovered via precipitation by adding water. XRD results indicated that the polymer did not intercalate into the vermiculite galleries implying that the flake morphology was fixed at the sonication stage. SEM and TEM confirmed the formation of bio-nanocomposites featuring a mixed morphology. The flakes were randomly distributed in the matrix and featured thicknesses ranging from submicron in size down into the nano-range. BET surface area measurement support flake thickness values below 100 nm. Good adhesion between the matrix and the flakes was indicted by fact that cryo-fracturing resulted in cohesive rather than adhesive failure at the flake surface. Adding 30 wt.% filler increased the melt viscosity, measured at 160 °C, by factor of about 20. It also doubled the tensile strength but decreased

the elongation-to-break by a factor of ten. Halpin-Tsai analysis of the variation in Young's modulus with filler content supported the high aspect ratio nature of the flake reinforcement. Dynamic mechanical analysis showed that the glass transition temperature (*T*g) of the polymer increased by up to 10 °C when the filler was added. This indicates that the high contact surface area presented by the dispersed nano-platelets dispersed in the matrix inhibited segmental polymer chain mobility. This implies an effective stiffening of the polymer matrix at temperatures above *T*g. It also explains, in part, the higher apparent reinforcing effect observed at temperatures above *T*g. Analysis of the variation in composite modulus with temperature and composition indicate that, below the glass transition temperature, the composite stiffness is adequately explained by invoking the reinforcing effect of the inorganic filler together with the apparent shift in *T*g. It is postulated that dynamic network formation through polymer-filler hydrogen bonding interactions provides a tertiary stiffening mechanism that operates at temperature above *T*g. In conclusion, the key finding of this work is that organo-modification of clays with surfactants is not essential for the preparation of polyamide-clay nanocomposites with excellent mechanical properties.

Acknowledgements

Financial support for this research from the National Research Foundation (NRF) via the South African/Algeria research partnership programme under Grant 87453 is gratefully acknowledged. Any opinion, finding and conclusion or recommendation expressed in this material is that of the authors and the NRF does not accept any liability in this regard.

References

[1] Fu SY, Feng XQ, Lauke B, Mai YW. Effects of particle size, particle/matrix interface adhesion and particle loading on mechanical properties of particulate-polymer composites. Composites Part B: Engineering. 2008;39(6):933-961.

[2] Yeh JT, Wang CK, Hu P, Lai YC, Huang LK, Tsai FC. Ultradrawing properties of ultrahigh-molecular-weight polyethylene/attapulgite fibers. Polymer International. 2012;61(6):982-989.

[3] Mago G, Kalyon DM, Fisher FT. Nanocomposites of polyamide-11 and carbon nanostructures: Development of microstructure and ultimate properties following solution processing. Journal of Polymer Science, Part B: Polymer Physics. 2011;49(18):1311-1321.

[4] Kiliaris P, Papaspyrides CD. Polymer/layered silicate (clay) nanocomposites: An overview of flame retardancy. Progress in Polymer Science (Oxford). 2010;35(7):902-958.

[5] Rodrigues LADS, Figueiras A, Veiga F, de Freitas RM, Nunes LCC, da Silva Filho EC, et al. The systems containing clays and clay minerals from modified drug release: A review. Colloids and Surfaces B: Biointerfaces. 2013;103:642-651.

[6] Arora A, Padua GW. Review: Nanocomposites in food packaging. Journal of Food Science. 2010;75(1):R43-R49.

[7] Utracki LA. Polymeric nanocomposites: Compounding and performance. Journal of Nanoscience and Nanotechnology. 2008;8(4):1582-1596.

[8] de Paiva LB, Morales AR, Valenzuela Díaz FR. Organoclays: Properties, preparation and applications. Applied Clay Science. 2008;42(1-2):8-24.

[9] Lebaron PC, Wang Z, Pinnavaia TJ. Polymer-layered silicate nanocomposites: An overview. Applied Clay Science. 1999;15(1-2):11-29.

[10] Pavlidou S, Papaspyrides CD. A review on polymer-layered silicate nanocomposites. Progress in Polymer Science (Oxford). 2008;33(12):1119-1198.

[11] Macheca A, Gnanasekaran D, Focke W. Surfactant-free dimer fatty acid polyamide/montmorillonite bio-nanocomposites. Colloid and Polymer Science. 2014;292(3):669-676.

[12] Fan XD, Deng Y, Waterhouse J, Pfromm P. Synthesis and characterization of polyamide resins from soy-based dimer acids and different amides. Journal of Applied Polymer Science. 1998;68(2):305-314.

[13] Walker GF, Garrett WG. Chemical Exfoliation of Vermiculite and the Production of Colloidal Dispersions. Science. 1967;156(3773):385-387.

[14] Muiambo HF, Focke WW, Atanasova M, der Westhuizen IV, Tiedt LR. Thermal properties of sodium-exchanged palabora vermiculite. Applied Clay Science. 2010;50(1):51-57.

[15] Muiambo HF, Focke WW, Atanasova M, Benhamida A. Characterization of urea-modified Palabora vermiculite. Applied Clay Science. 2015;105–106(0):14-20.

[16] Justo A, Maqueda C, Perez-Rodríguez JL, Morillo E. Expansibility of some vermiculites. Applied Clay Science. 1989;4(5-6):509-519.

[17] Hillier S, Marwa EMM, Rice CM. On the mechanism of exfoliation of 'Vermiculite'. Clay Minerals. 2013;48(4):563-582.

[18] Kehal M, Reinert L, Duclaux L. Characterization and boron adsorption capacity of vermiculite modified by thermal shock or H2O2 reaction and/or sonication. Applied Clay Science. 2010;48(4):561-568.

[19] Obut A, Girgin I. Hydrogen peroxide exfoliation of vermiculite and phlogopite. Minerals Engineering. 2002;15(9):683-687.

[20] Marwa EMM, Meharg AA, Rice CM. The effect of heating temperature on the properties of vermiculites from Tanzania with respect to potential agronomic applications. Applied Clay Science. 2009;43(3-4):376-382.

[21] Wiewióra A, Pérez-Rodríguez JL, Perez-Maqueda LA, Drapała J. Particle size distribution in sonicated high- and low-charge vermiculites. Applied Clay Science. 2003;24(1-2):51-58.

[22] Poyato J, Pérez-Rodríguez JL, Ramírez-Valle V, Lerf A, Wagner FE. Sonication induced redox reactions of the Ojén (Andalucía, Spain) vermiculite. Ultrasonics Sonochemistry. 2009;16(4):570-576.

[23] Pérez-Maqueda LA, Canea OB, Poyato J, Pérez-Rodríguez JL. Preparation and characterization of micron and submicron-sized vermiculite. Physics and Chemistry of Minerals. 2001;28(1):61-66.

[24] Pérez-Rodríguez JL, Carrera F, Poyato J, Pérez-Maqueda LA. Sonication as a tool for preparing nanometric vermiculite particles. Nanotechnology. 2002;13(3):382-387.

[25] Ali F, Reinert L, Levêque J-M, Duclaux L, Muller F, Saeed S, et al. Effect of sonication conditions: Solvent, time, temperature and reactor type on the preparation of micron sized vermiculite particles. Ultrasonics Sonochemistry. 2014;21(3):1002-1009.

[26] Yao Y, Lu GQ, Boroyevich D, Ngo KDT. Survey of high-temperature polymeric encapsulants for power electronics packaging. IEEE Transactions on Components, Packaging and Manufacturing Technology. 2015;5(2):168-181.

[27] Schwellnus CM. Vermiculite Deposits in the Palaboroa Area, N.E. Transvaal. Pretoria: Government Printer; 1938.

[28] Basset WA. The Geology of Vermiculite Occurrences. Clays and Clay Minerals. 1961;10(1):61-69.

[29] Schoeman JJ. Mica and vermiculite in South Africa. Journal of The South African Institute of Mining and Metallurgy. 1989;89(1):1-12.

[30] Folorunso O, Dodds C, Dimitrakis G, Kingman S. Continuous energy efficient exfoliation of vermiculite through microwave heating. International Journal of Mineral Processing. 2012;114–117:69-79.

[31] Mathieson AM. Mg-vermiculite: A refinement of the crystal structure of the 14.36 Å phase. American Mineralogist. 1958;43:216-227.

[32] Newman ACD, Brown G. The chemical constitution of clays. In: Newman ACD, editor. Chemistry of Clays and Clay Minerals. London: Longman Scientific & Technical Mineralogical Society; 1987. p. 1-128.

[33] Ruiz Amil A, F.; AdlC, Vila E, Ruiz Conde A. Study of a material from Libby, Montana containing vermiculite and hydrobiotite; intercalation with aliphatic amines. Clay Minerals. 1992;27:257-263.

[34] Qian Y, Lindsay CI, Macosko C, Stein A. Synthesis and Properties of Vermiculite-Reinforced Polyurethane Nanocomposites. ACS Applied Materials & Interfaces. 2011;3(9):3709-3717.

[35] Carvalho HWP, Santilli CV, Briois V, Pulcinelli SH. Polymer-clay nanocomposites thermal stability: experimental evidence of the radical trapping effect. RSC Advances. 2013;3(45):22830-22833.

[36] Halpin JC, Kardos JL. HALPIN-TSAI EQUATIONS: A REVIEW. Polymer Engineering and Science. 1976;16(5):344-352.

[37] Tucker Iii CL, Liang E. Stiffness predictions for unidirectional short-fiber composites: Review and evaluation. Composites Science and Technology. 1999;59(5):655-671.

[38] Fornes TD, Paul DR. Formation and properties of nylon 6 nanocomposites. Polímeros. 2003;13:212-217.

[39] van Es MA. Polymer-clay nanocomposites, the importance of particle dimensions [PhD]. Delft, The Netherlands: Delft University of Technology; 2001.

[40] Suk JW, Piner RD, An J, Ruoff RS. Evaluation of elastic modulus of ultra-thin vermiculite membranes by contact mode atomic force microscopy imaging. Thin Solid Films. 2013;527:205-209.

[41] Sinha Ray S, Okamoto M. Polymer/layered silicate nanocomposites: a review from preparation to processing. Progress in Polymer Science. 2003;28(11):1539-1641.

[42] Wagener R, Reisinger TJG. A rheological method to compare the degree of exfoliation of nanocomposites. Polymer. 2003;44(24):7513-7518.

[43] Hablot E, Matadi R, Ahzi S, Vaudemond R, Ruch D, Avérous L. Yield behaviour of renewable biocomposites of dimer fatty acid-based polyamides with cellulose fibres. Composites Science and Technology. 2010;70(3):525-529.